Astrophysical Journal, in press

The Symmetric parsec-scale Jets of the Radio Galaxy Hydra A

Gregory B. Taylor
NRAO, P.O. Box 0, Socorro, NM 87801

ABSTRACT

Sensitive, high-resolution VLBA observations of the nuclear region of the radio galaxy Hydra A are presented at 1.3, 5 and 15 GHz. These observations reveal a surprising degree of symmetry in the central 100 mas (140 pc). Jet-to-counterjet ratios at all three frequencies are in the range 1.1 – 1.2. The VLBI jets are straight and well aligned with the inner VLA jets at 1.3 and 5 GHz, but there is a 6° bend in the inner jet axis visible in the highest resolution 15 GHz image. There is strong evidence that the core and inner jets are free-free absorbed by an ionized gas with a density of 300 cm^{-3}. Hydra A is also unusual in that the 21 cm atomic Hydrogen line is seen in absorption against the nucleus. I present VLBA observations that spatially and spectrally resolve the HI in absorption against the inner nucleus and jets. This gas is most likely distributed in a disk having a rotation axis closely aligned with the jet axis and with a height of ∼30 pc.

Subject headings: galaxies:active — galaxies:individual (Hydra A) — radio continuum:galaxies — radio lines:general

1. Introduction

Hydra A (3C 218) is an outstanding example of a high-luminosity FRI radio galaxy. It has a total angular extent of 8′, although at frequencies of 5 GHz and above only the central few arcminutes are readily imaged (Taylor *et al.* 1990). The source morphology has a high degree of 'S' symmetry, which Taylor *et al.* suggest may be due to precession of the central engine. The host galaxy has been identified with a cD galaxy (Matthews, Morgan & Schmidt 1964) having a double optical nucleus (Ekers & Simkin 1983). Observations of nuclear optical emission lines (Simkin 1979, Hansen, Jorgensen & Norgaard-Nielsen 1995) reveal a disk of gas with a rotation axis of 29° ± 9°. This rotation axis is nearly parallel to the kpc-scale jet axis of $\sim 26°$(Taylor *et al.* 1990), and nearly perpendicular to the direction of the secondary nucleus which is 10″ from the primary optical nucleus at a position angle of 125°.

The Hydra A galaxy is the dominant member of the Abell cluster A780. This cluster is a strong source of X-ray emission and has been classified as a cooling flow cluster with a mass accretion rate of 600 $M_{\odot}yr^{-1}$(David *et al.* 1990). Taylor & Perley (1993) have demonstrated extremely high (> 8000 radians m^{-2}) Faraday rotation measures (RMs) and a striking RM and depolarization asymmetry between the northern and southern radio lobes, with the southern lobe having substantially greater RMs and depolarization. They suggest the most likely mechanism to produce the high RMs is a magnetized cluster gas. The asymmetry between the north and south lobes can then be understood as partly due to the orientation of the radio source such that the northern lobe is closer to us and hence the radiation from it passes through a more shallow Faraday screen. In view of this asymmetry and likely inclination of the source on the kpc-scale Hydra A appears remarkably symmetric on the pc-scale in the radio continuum.

I assume H_0 = 50 km s^{-1} Mpc^{-1} throughout, so at the redshift of Hydra A of 0.05424 (see §3.3), 1 mas corresponds to 1.44 pc.

2. Observations

The observations were carried out at 1.347, 4.991, and 15.36 GHz using the 10 element VLBA of the NRAO[1] on 1995 March 17-18. Integration times are given in Table 1. Both right and left circular polarizations were recorded using 2 bit sampling across a total bandwidth of 8 MHz. Following correlation, global fringe fitting was performed using the AIPS task FRING, an implementation of the Schwab & Cotton (1983) algorithm. The fringe fitting was performed using a solution interval of 6.5 minutes and with the assumption of a point source model. Once delay and rate solutions had been applied the data were averaged in frequency over 8 MHz. 3C 84 was used for bandpass calibration of the 1.347 GHz data. In fact the observations of 3C 84 at this frequency, resolution and sensitivity were sufficiently interesting to warrant a separate paper (Taylor & Vermeulen 1996).

Amplitude calibration for each antenna was derived from measurements of the antenna gain and system temperature during each run. In addition, the strong calibrator DA193 (0552+398) was observed to refine the amplitude calibration. Strong interference at 1.347 GHz at Saint Croix, probably due to FAA radar transmissions from Pico Del Este at 1.35 GHz (Bagri 1992), resulted in the loss of 26 minutes of data from this station. Otherwise the performance of all 10 VLBA stations was excellent. All editing, imaging, deconvolution, and self-calibration were performed

[1]The National Radio Astronomy Observatory is operated by Associated Universities, Inc., under cooperative agreement with the National Science Foundation

using DIFMAP (Shepherd, Pearson & Taylor 1995). The two hands of polarization were added together for imaging, but were left separate in the self-calibration.

3. Results and Discussion

3.1. Symmetry of the inner jets

Fig. 1a shows the 1.3 GHz VLBA image of the nucleus of Hydra A at $\sim$10 mas resolution. The jet is straight along a position angle of 23° and symmetric about the core with a jet-to-counterjet ratio of 1.2. The northern side, being slightly stronger, is denoted the "jet" side, and the weaker southern jet the "counterjet" side. The jet-to-counterjet ratios are taken from the integrated flux ratios after removal of the core component (see Table 2). Fig. 1b shows the 5 GHz VLBA image of the nucleus of Hydra A at $\sim$2 mas resolution. The jet at this frequency also appears straight along a position angle of 23° and symmetric about the core with a jet-to-counterjet ratio of 1.12. Fig. 1c shows the 15 GHz VLBA image at a resolution of $\sim$1 mas. The inner jet seen at 15 GHz is oriented along a position angle of 17°, and gradually curves to match the position angle of 23° seen at both 1.3 and 5 GHz. The jet-to-counterjet ratio at 15 GHz is 1.15.

For two oppositely directed relativistic jets moving away from a common origin along an axis at an angle θ to the line-of-sight, the jet-to-counterjet ratio, R, due to Doppler beaming effects is given by

$$R = \left(\frac{1+\beta\cos\theta}{1-\beta\cos\theta}\right)^{k-\alpha} \tag{1}$$

where β is the bulk velocity of the jet in units of v/c, α is the spectral index defined $S_\nu \propto \nu^\alpha$, and $k=2$ for a continuous jet or $k=3$ for discrete jet components.

Hydra A is only the second FRI source, the first being 3C 338 (Feretti *et al.* 1993), discovered to have pc-scale jets on *both* sides of of the central engine. Interestingly enough, both are among the small number of radio sources associated with the dominant galaxy in a cooling flow cluster (Taylor, Baron & Ge 1994). For Hydra A, the jet-to-counterjet ratio of 1.2 implies, from Eq.(1), that $\beta\cos(\theta) = 0.03$ for a continuous ($k = 2$) jet. Thus if all jets start out relativistic, then the jet in Hydra A must be oriented within $<$2° of the plane of the sky. Observations of the large-scale RM asymmetries in Hydra A, however, predict an inclination angle of 48°(Taylor & Perley 1993). While this discrepancy can be explained by a large bend between the inner jet and the lobes, this seems unlikely given the good agreement between the projected pc and kpc scale jet axis. Alternatively, the inner jets could be aligned with the outer jets at an inclination of 48°, and the bulk jet velocity could be low ($\beta = 0.05$). It has been suggested (e.g. Soker & Sarazin 1988, Sulkanen, Burns & Norman 1989) that cooling flows may decelerate the radio jets, although such disruption has been considered to occur at the sonic radius somewhere between 0.1–10 kpc. Unless the cooling flows have an affect on the jet closer to the nucleus than previously thought it is difficult to understand why the pc-scale jets in Hydra A and 3C 338 would have such low bulk velocities. On the kpc scale, the jet-to-counterjet ratio at 5 GHz is 1.9. It could also be that the jets of Hydra A are influenced more by interactions with the surrounding medium than by Doppler boosting effects.

3.2. Spectral Indices and the Low-Frequency Cutoff

By tapering the higher frequency images, I have made spectral index maps between 5 and 15 GHz and between 1.3 and 5 GHz (Fig. 2). It is important to note that spectral index maps made from two datasets with substantially different u-v coverages (such as are presented here) may suffer from significant systematic errors. Nevertheless I believe the maps here to be representative of the trends in the nucleus of Hydra A. Both frequency pairs reveal steep spectrum jets emerging on both sides of an inverted spectrum core.

The overall spectrum of the nucleus of Hydra A from VLA observations (Taylor *et al.* 1990, Taylor 1991) from 330 MHz to 15 GHz is shown in Fig. 3. From the VLBA observations, which recover nearly all the flux seen by the VLA, I have decomposed the spectrum into the unresolved emission from the central core component, and the total jet emission from the inner 20 mas (Table 2). The core emission is seen to be inverted, while the jet emission peaks at $\sim$5 GHz. The low-frequency turnover of the jet emission could be the result of synchrotron self-absorption or free-free absorption by thermal gas in the vicinity of the nucleus. Synchrotron self-absorption seems unlikely since the predicted turnover in the spectrum of a component with a flux density of 50 mJy and a size of 2 mas, assuming equipartition conditions apply, is 100 MHz (Scott & Readhead 1977). Unless there is considerable sub-structure in the jets, or conditions very far out of equipartition (field strengths greater by over 6 orders of magnitude) synchrotron self-absorption cannot reproduce the observed turnover in the spectrum around 5 GHz. A more likely explanation is free-free absorption by a thermal gas in the nuclear region. For a pure H plasma the free-free optical depth is given by Levinson, Laor & Vermeulen 1995 to be:

$$\tau_{\rm ff} \simeq 5 \times 10^{-8}\, T_4^{-3/2}\, n_{\rm e}^2\, \nu_9^{-2}\, g\, d_{\rm pc}, \tag{2}$$

where $d_{\rm pc}$ is the path length through the absorbing medium in parsecs, T_4 is the gas temperature in units of 10^4K, $n_{\rm e}$ is the electron density in cm^{-3}, ν_9 is the frequency in GHz, and g is the thermal average Gaunt factor which is of order 5 for $T_4 = 1$ and $\nu_9 = 1.3$ (Spitzer 1978). Extrapolating the jet flux observed at 15 GHz to 1.3 GHz assuming a spectral index of -0.7 gives an optical depth of 1.2 to reproduce the observed flux density at 1.3 GHz. Assuming $T_4 = 1$, and a path length of $d_{\rm pc} = 100$, requires a density of 300 cm^{-3} to produce this optical depth. If this gas is uniformly distributed, then the total mass requirement is 3×10^7 M$_\odot$. This mass can be reduced by lowering its temperature or confining the gas to a smaller, higher density, region around the radio jets.

3.3. The HI absorbing gas

HI was discovered in absorption towards the nucleus of Hydra A on 1991 May 5. The observations were made using the VLA in its D-configuration for 7 hours. Even after bandpass calibration using the strong continuum source 3C 273, a time-dependent ripple with a wavelength of 3 MHz remained present in the data (this well known standing wave effect at the VLA has been described by Carilli 1991). This slow variation was removed by fitting a 6th order Chebyshev polynomial to the data. The final resulting spectrum is shown in Fig. 4. Prior to fitting a continuum flux density of 24.65 Jy was subtracted. The maximum absorption of 32 mJy/beam occurs at a redshift of 0.05424 $\pm$ 0.00007. The systemic redshift from optical observations of the nucleus has been given as 0.0542 $\pm$ 0.0001 (Dwarakanath, Owen & van Gorkom 1995, Owen, Ledlow & Keel 1995), and 0.0546 $\pm$ 0.0003 (Hansen, Jorgensen & Norgaard-Nielsen 1995). Given the errors in determining the optical redshift, the HI absorption and the systemic optical velocity are in agreement. The optical depth in the HI line of these VLA observations is 0.0015, although it was immediately recognized that this low optical depth was due to dilution by the strong lobe components entering the 45$''$ synthesised beam (Taylor 1991). No HI was detected in emission. The 6σ upper limit of <30 mJy/beam corresponds to an HI mass per beam of $< 120 \times 10^7$ M$_\odot$, for a line width of 22 km s^{-1}. In deriving such a limit for a typical galaxy one would generally integrate over a wider velocity range, however the strong and complicated continuum emission present in Hydra A limits the dynamic range such that the sensitivity to HI in emission actually decreases with greater averaging in velocity.

Dwarakanath, van Gorkom & Owen 1994 performed VLA B-configuration observations of three cooling flow clusters with embedded radio sources, including Abell 780 containing Hydra A, and confirmed the detection of HI gas in absorption. Follow-up VLA A-configuration observations with higher spatial and spectral resolution are reported in Dwarakanath, Owen & van Gorkom 1995, who also place limits on the optical depth of HI against the lobes of <0.007. Based on the strong HI absorption detected towards the nucleus and the lack of HI absorption occurring toward any other region of the radio source, they suggest that the HI gas is distributed in a disk within the central few kpc of the galaxy.

I present spatially resolved HI absorption detected against the core and parsec scale jets of Hydra A (Fig. 5). The two spectra from the northern and southern jet are separated by 23 mas (33 pc), and show absorption peaks shifted by 20 km s^{-1}. The absorption to both the north and south is also considerably more narrow ($\sim$35 km s^{-1}) than towards the core ($\sim$80 km s^{-1}). This is also evident in the individual channel maps shown with the continuum subtracted in Fig. 6. While the central velocity of the core component occurs at 16271 km s^{-1}, the southern lobe shows up most clearly in absorption at 16277 – 16284 km s^{-1} and the northern jet between 16258 – 16269 km s^{-1}. The optical depths and column densities towards the three components are listed in Table 3. Lower limits on the total mass of the absorbing gas are also estimated in Table 3 from:

$$M_{\rm HI} \simeq 8\, N_{21}\, A_{\rm pc^2}\, h^{-2}\, {\rm M}_\odot, \qquad (3)$$

where N_{21} is the HI column density in units of 10^{21} cm^{-2}, and A is the area of the region absorbed in pc^2. The area is taken to be roughly the beamsize since the components are only marginally resolved at 1.3 GHz. The true source area is likely to be smaller and hence the HI masses derived are upper limits. These masses are comparable to those of typical HI clouds in our own galaxy (Spitzer 1978), and are much lower than can be detected in emission in other galaxies using current techniques. The HI density in front of the core, assuming a path length of 10 pc, is 450 cm^{-3}, similar to the thermal gas density needed to produce the low frequency turnover by free-free absorption (see §3.2).

The HI absorbing gas could be (1) falling into the nucleus, (2) contained within one or more clouds passing in front of the nucleus, or (3) distributed in a disk. The first possibility is unlikely because if this were the case then the HI gas should be seen redshifted with respect to the optical velocity, and the observed shift is < 90 km s^{-1}. The second possibility also seems unlikely based on the greater optical depth and dispersion velocity seen towards the core. A disk also has the advantage that it would be more persistent than a passing cloud. Below I consider the possibility of HI distributed in a disk. The present observations provide some constraints on the kinematics of the HI disk. The rotation axis of the disk cannot be precisely coincident with the jet axis since we see a shift of 20 km s^{-1} between the north and south HI absorption peaks. Unfortunately the velocity gradient along the disk is unknown since the core is unresolved. Assuming a simple solid body rotation for the disk, the minimum gradient, estimated by dividing the total velocity span of 120 km s^{-1} by the east-west beam size (9 pc), is 13 km s^{-1} pc $^{-1}/\sin(i)$, where i is the inclination of the disk. This leads to a maximum difference between the rotation axis of the disk and the jet axis of 6°. Taking the inclination of the disk to be 48°(see §3.1), and the size of the core to be 9 pc, then I derive the mass within the central 5 pc to be 10^7 M$_\odot$. This estimate, however, depends critically on the geometry of the continuum source and the absorbing material. If the HI gas is distributed in a torus much larger than the core, then the absorption may only be sampling the velocities transverse to our line-of-sight, causing the mass of the central region to be severly underestimated. Given that the optical depth in the central 50 km s^{-1} appears to decrease both to the north and south (Fig. 7), the thickness of the disk appears to be ∼30pc. The optical depth also seems to decrease more quickly to the north than to the south, which is consistent with the northern jet being pointed towards us.

The orientation of the pc-scale disk (23° ± 6°), is consistent with that of the kpc-scale disk observed in the optical (29° ± 9°– Simkin 1979, Hansen, Jorgensen & Norgaard-Nielsen 1995). The density of the optical emission line gas within the central kpc has been estimated to be 240 cm^{-3} (Heckman *et al.* 1995), which is only a factor of 2 less than the HI density derived above for the pc-scale disk. Thus there is plausible evidence for a disk in Hydra A extending from the central parsecs out to a few kiloparsecs in radius.

4. Conclusions

The parsec-scale jets of Hydra A appear surprisingly symmetric given the observed RM and depolarization asymmetries seen on larger scales. This may indicate that the emission observed from the jets is more dependent on interactions with the surrounding material than on Doppler boosting. Other evidence supporting a fairly dense nuclear environment is free-free absorption of the inner jets and core by a thermal gas with a density of 300 cm^{-3}, and HI absorption by a gas of similar density. The HI gas appears be be distributed in a disk with a total vertical extent $\sim$30 pc, and a rotation axis that is close (within 6°) to the jet axis of 23°. This rotation axis is also consistent with that of the kpc-scale disk seen in optical emission lines.

To establish better limits on the geometry and mass of the HI disk, more sensitive and higher resolution observations using a world array that includes the 10 VLBA stations and the 100-m antenna at Effelsberg are planned. Future VLB observations at 15 GHz would be useful to measure proper motions in the pc-scale jet and changes in the inner jet axis.

I thank Jacqueline van Gorkom for her encouragement of this project from the time of its conception in 1990 through all its many stages. I am also grateful to Rick Perley and Frazer Owen for useful discussions, and to the referee, Chris O'Dea, for insightful comments on the manuscript.

TABLE 1

VLBA Observational Parameters

Source (1)	Frequency (2)	BW (3)	$\Delta\nu$ (4)	Δt (5)	Scan (6)	Time (7)
Hydra A	15.36	8	125	2	13	2.4
	4.991	8	125	2	13	3.5
	1.347	8	15.6	4	13	2.1
3C 84	1.347	8	15.6	4	13	1.5

Notes to Table 1

Col.(1).—Source name. Col.(2).—Observing frequency in GHz. Col.(3).—Total spanned bandwidth in MHz. Col.(4).—Channel width output from correlator in kHz. Col.(5).—Integration time output from correlator in seconds. Col.(6).—Length of each scan in minutes. Col.(7).—Total integration time on source in hours.

TABLE 2

COMPONENT FLUX DENSITIES

Component	$S_{15\mathrm{GHz}}$ (mJy)	$S_{5\mathrm{GHz}}$ (mJy)	$S_{1.3\mathrm{GHz}}$ (mJy)	α_{5-15}	$\alpha_{1.3-5}$
N. jet	39 ± 2	74 ± 4	48 ± 5	-0.60	0.33
core	127 ± 6	103 ± 5	40 ± 4	0.19	0.72
S. Jet	34 ± 2	66 ± 4	40 ± 4	-0.59	0.38

Note – The flux densities reported here for the north and south jets are for the inner jets, at a distance of $\sim$10 mas from the core. These components are not well resolved in the the 1.3 GHz data.

TABLE 3

HI Column Densities and Masses

Component	S_{cont}	τ	V	ΔV	N_{HI}	Area	M_{HI}
(1)	(2)	(3)	(4)	(5)	(6)	(7)	(8)
N. jet	16	0.46	16265	38	2.0×10^{21}	200	3200
core	85	0.99	16271	78	14.0×10^{21}	200	22000
S. Jet	19	0.55	16279	57	5.7×10^{21}	200	9100

Notes to Table 3

Col.(1).—Component location. Col.(2).—Continuum flux density in mJy. Col.(3).—Optical depth. Col.(4).—Central velocity in km s^{-1}. Col.(5).—FWHM in velocity in km s^{-1}. Col.(6).—The column density in units of cm^{-2} calculated assuming a spin temperature, T_s, of 100 K. Col.(7).—The area covered by the component in pc^2. Col.(8).—The HI mass estimated from Eq.(3) in solar masses.

REFERENCES

Bagri, D.S. (1992) VLA - VLBA Interference Memorandum, No. 2, 1

Carilli, C. L. (1991) VLA Test Memorandum, No. 158, 1

David, L.P., Arnaud, K.A., Forman, W., & Jones, C. (1990) ApJ, 356, 32

Dwarakanath, K.S., van Gorkom, J.H., & Owen, F.N. (1994) ApJ, 432, 469

Dwarakanath, K.S., Owen, F.N., & van Gorkom, J.H. (1995) ApJL, 442, L1

Ekers, R. D., Simkin, S. M. (1983) ApJ, 265, 85

Feretti, L., Comoretto, G., Giovannini, G., Venturi, T., & Wehrle, A.E. (1993) ApJ, 408, 446

Hansen, L., Jorgensen, H.E., Norgaard-Nielsen, H.O. (1995) A&A, 301, 640

Heckman, T.M., Baum, S.A., van Breugel, W.J.M., & McCarthy, P. (1989) ApJ, 338, 48

Levinson, A., Laor, A., & Vermeulen, R.C. (1995) ApJ, 448, 589

Matthews, T.A., Morgan, W.W. Schmidt, M. (1964) ApJ, 140, 35

Owen, F.N., Ledlow, M.J., & Keel, W.C. (1995) AJ, 109, 14

Schwab, F.R., & Cotton, W.D. (1983) AJ, 88, 688

Scott, M.A., & Readhead, A.C.S. (1977) MNRAS, 180, 539

Shepherd, M.C., Pearson, T.J., & Taylor, G.B. (1995) BAAS, 27, 903

Simkin, S. M. (1979) ApJ, 234, 56

Soker, N., & Sarazin, C.L. (1988) ApJ, 327, 66

Spitzer, L. (1978) *Physical Processes in the Interstellar Medium*, (New York:Wiley)

Sulkanen, M.E., Burns, J.O., & Norman, M.L. (1989) ApJ, 344, 604

Taylor, G.B., Perley, R.A., Inoue, M., Kato, T., Tabara, H., & Aizu, K. (1990) ApJ, 360, 41

Taylor, G.B. (1991) Ph.D. Thesis, University of California, Los Angeles

Taylor, G.B., & Perley, R.A. (1993) ApJ, 416, 554

Taylor, G.B., Barton, E.J., & Ge, J.-P. (1994) AJ, 107, 1942

Taylor, G.B., & Vermeulen, R.C. (1996) ApJL, 457, L69

This preprint was prepared with the AAS LaTeX macros v4.0.

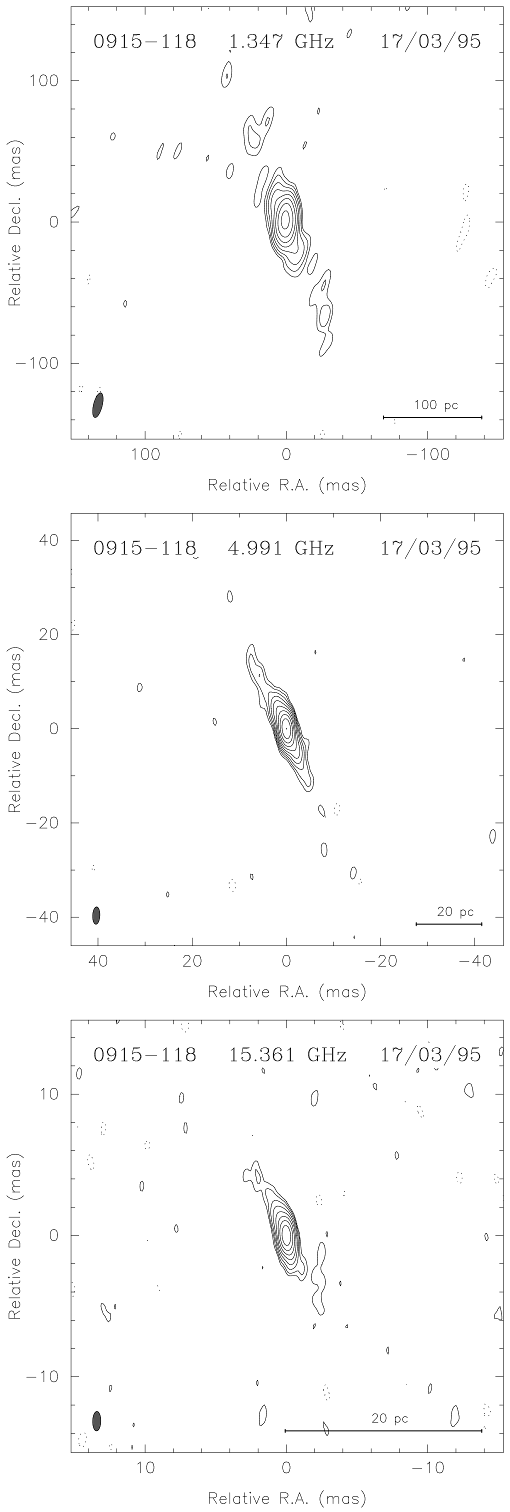

Fig. 1.— **a.** The nucleus of Hydra A at 1.3 GHz. Contours are drawn at −0.5, 0.5, 1, 2, 4, 8, 16, 32, and 64 mJy/beam where the beamsize is 17.9 × 6.2 mas in p.a. −14°. **b.** The nucleus of Hydra A at 5 GHz. Contours are drawn at −0.3, 0.3, 0.6, 1.2, 2.4, 4.8, 9.6, 19.2, 38, 77, and 154 mJy/beam where the beamsize is 3.66 × 1.53 mas in p.a. −3°. **c.** The nucleus of Hydra A at 15 GHz. Contours are at −0.6, 0.6, 1.2, 2.4, 4.8, 9.6, 19.2, 38, and 77 mJy/beam where the beamsize is 1.38 × 0.58 mas in p.a. −1°.

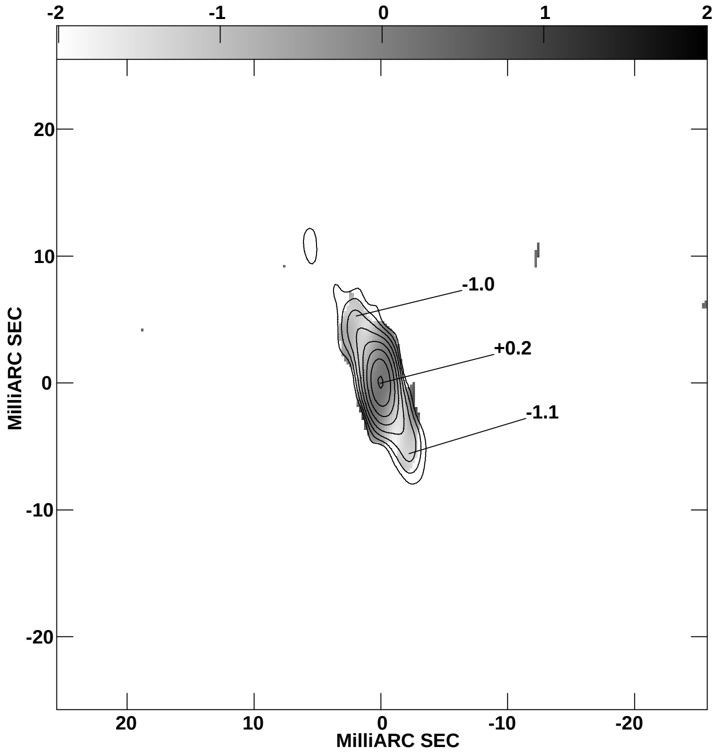

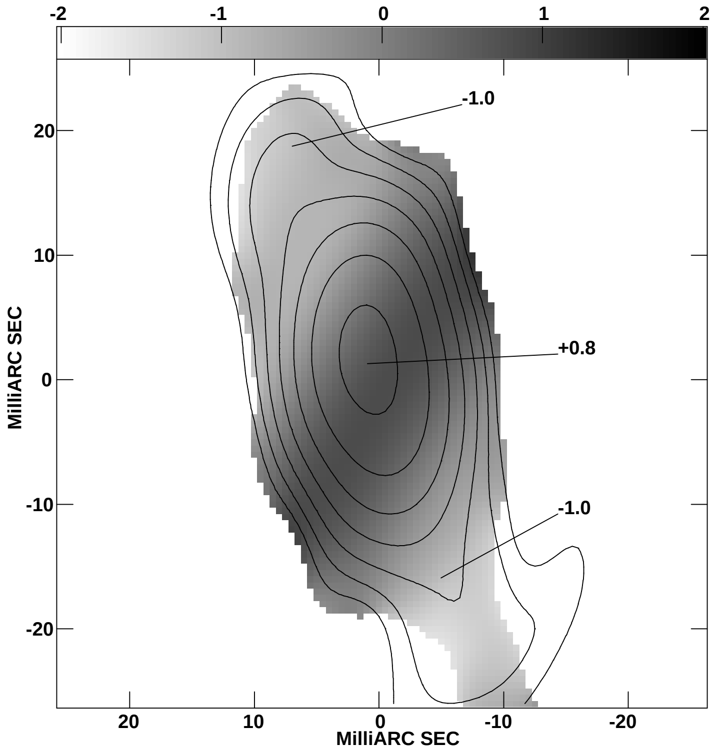

Fig. 2.— **a.** The spectral index map of Hydra A between 5 and 15 GHz. The 15 GHz data has been tapered and restored with the same beam as the 5 GHz data of 3.1×1.2 mas in p.a. $-6°$. Contours are from the 5 GHz image at 1, 2, 4, 8, 16, 32, 64 and 128 mJy/beam. **b.** The spectral index map of Hydra A between 1.3 and 5 GHz. The 5 GHz data has been tapered and restored with the same beam as the 1.3 GHz data of 12×6 mas in p.a. $-14°$. Contours are from the 1.3 GHz image at 1, 2, 4, 8, 16, 32, and 64 mJy/beam.

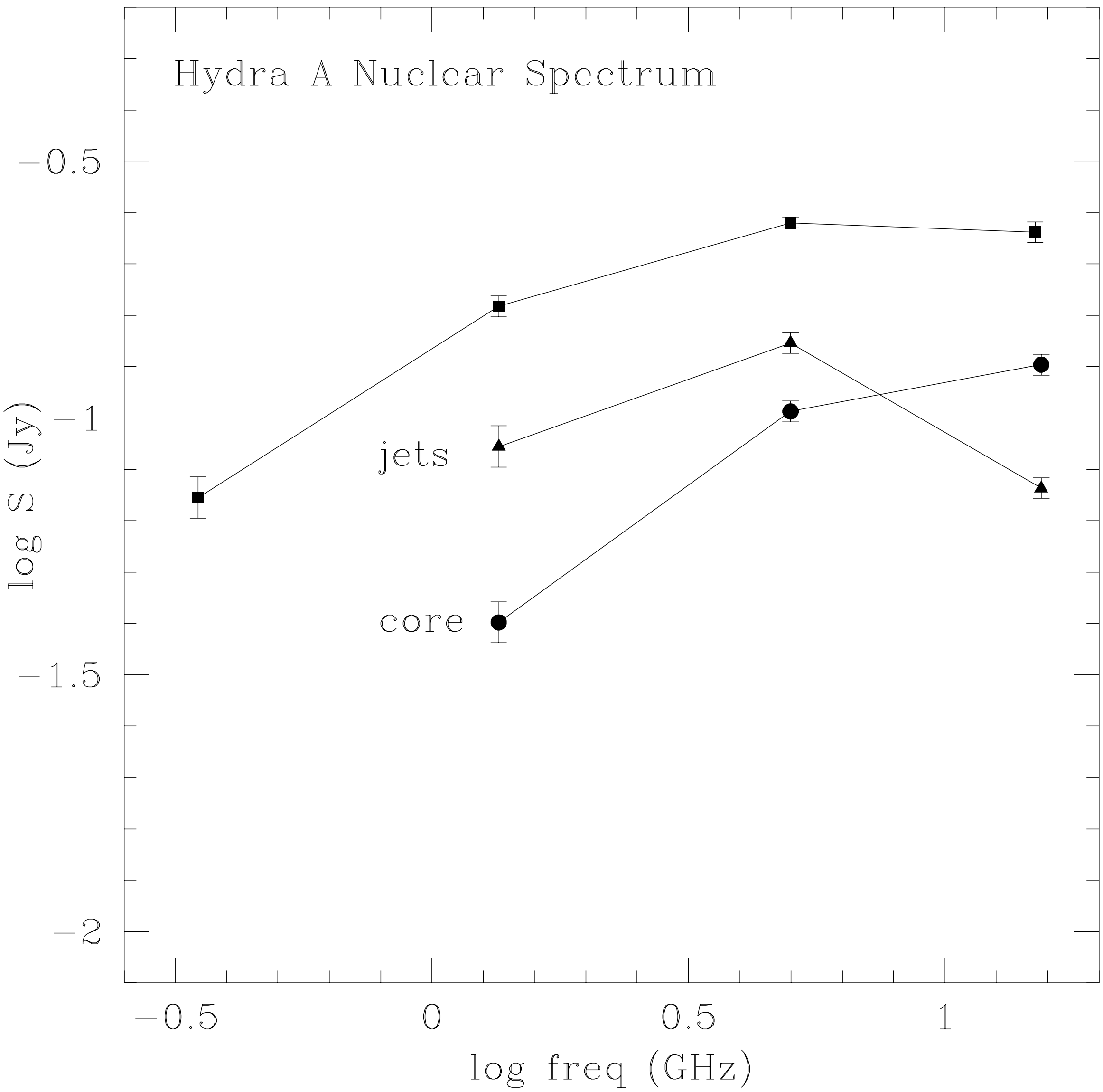

Fig. 3.— The nuclear spectrum of Hydra A and its constituents. The square symbols represent VLA measurements of the total nuclear emission from Hydra A. The triangles and circles indicate measurements of the flux density contained in the nuclear jets and unresolved core respectively.

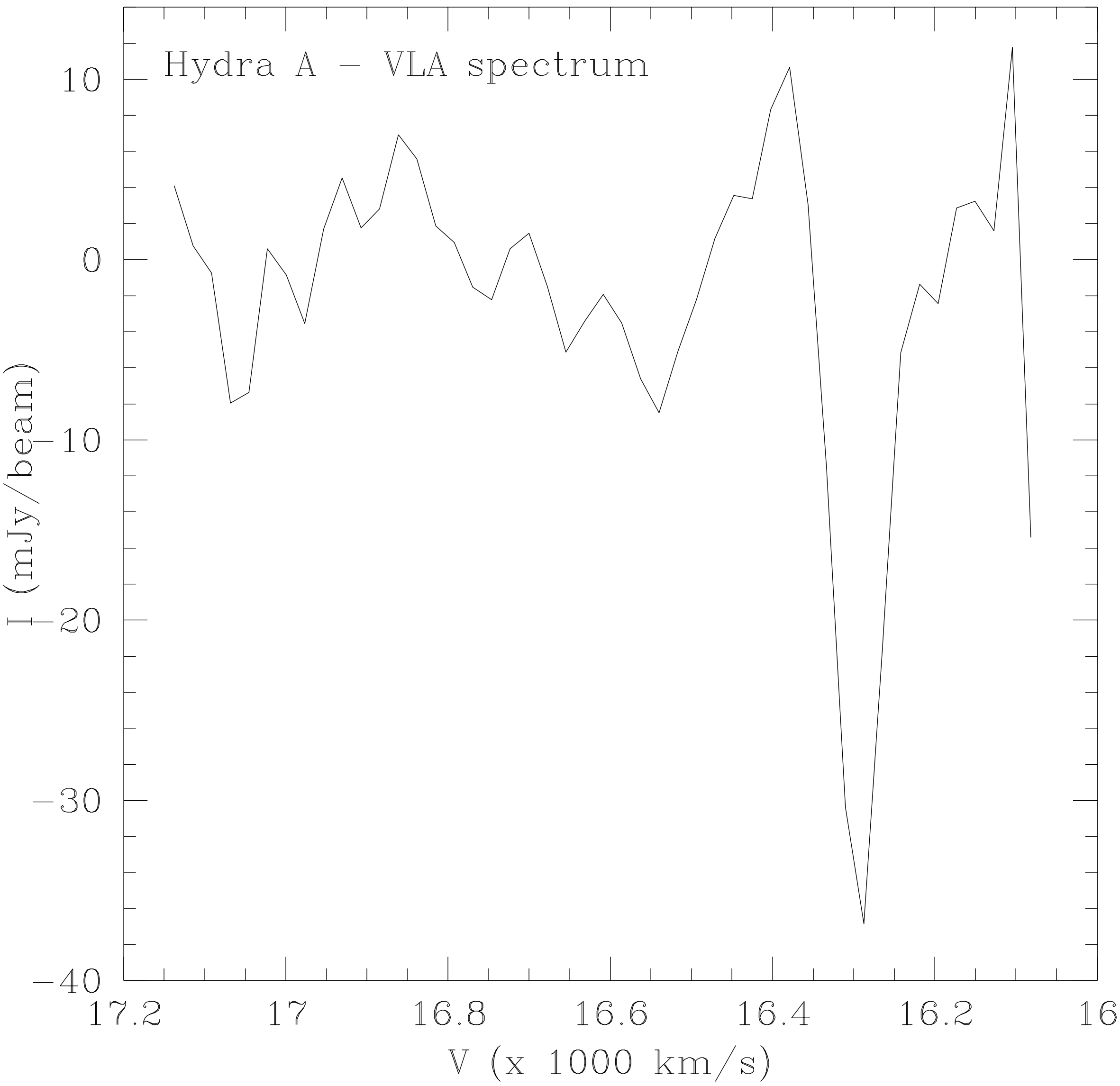

Fig. 4.— The discovery spectrum of HI absorption against the nucleus of Hydra A. These observations were made using the VLA in the D configuration with a beam size of 45″. The total velocity spanned is 1100 km s^{-1} with a spectral resolution of 22 km s^{-1}. A continuum flux density of 24.65 Jy has been subtracted.

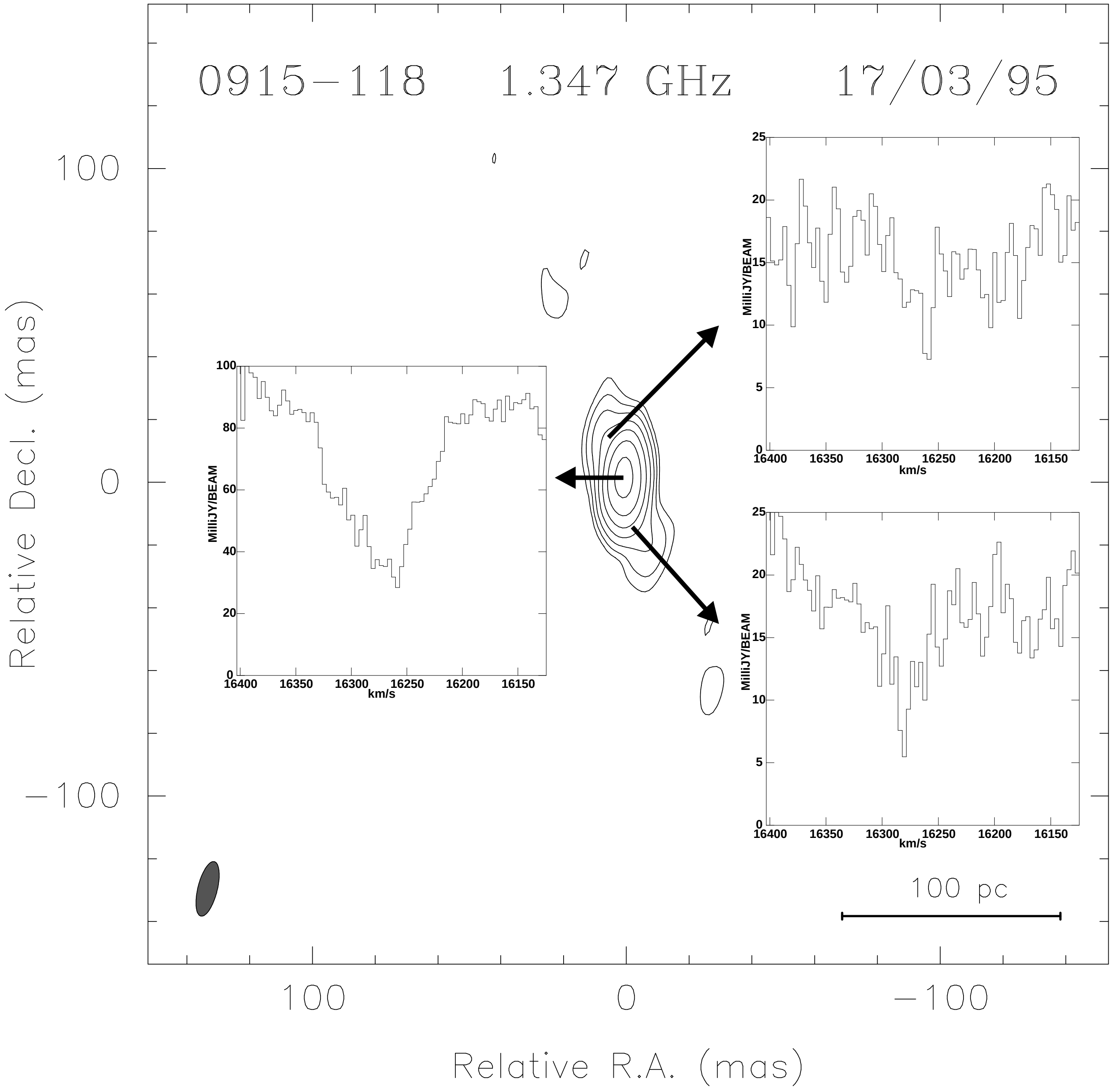

Fig. 5.— HI absorption at selected locations in the nucleus of Hydra A. Contours are from the 1.3 GHz continuum image at −1, 1, 2, 4, 8, 16, 32, and 64 mJy/beam with a beam size of 18 × 6 mas in p.a. −14°. The total velocity spanned by the inset figures is 250 km s^{-1} with a spectral resolution of 3.67 km s^{-1}.

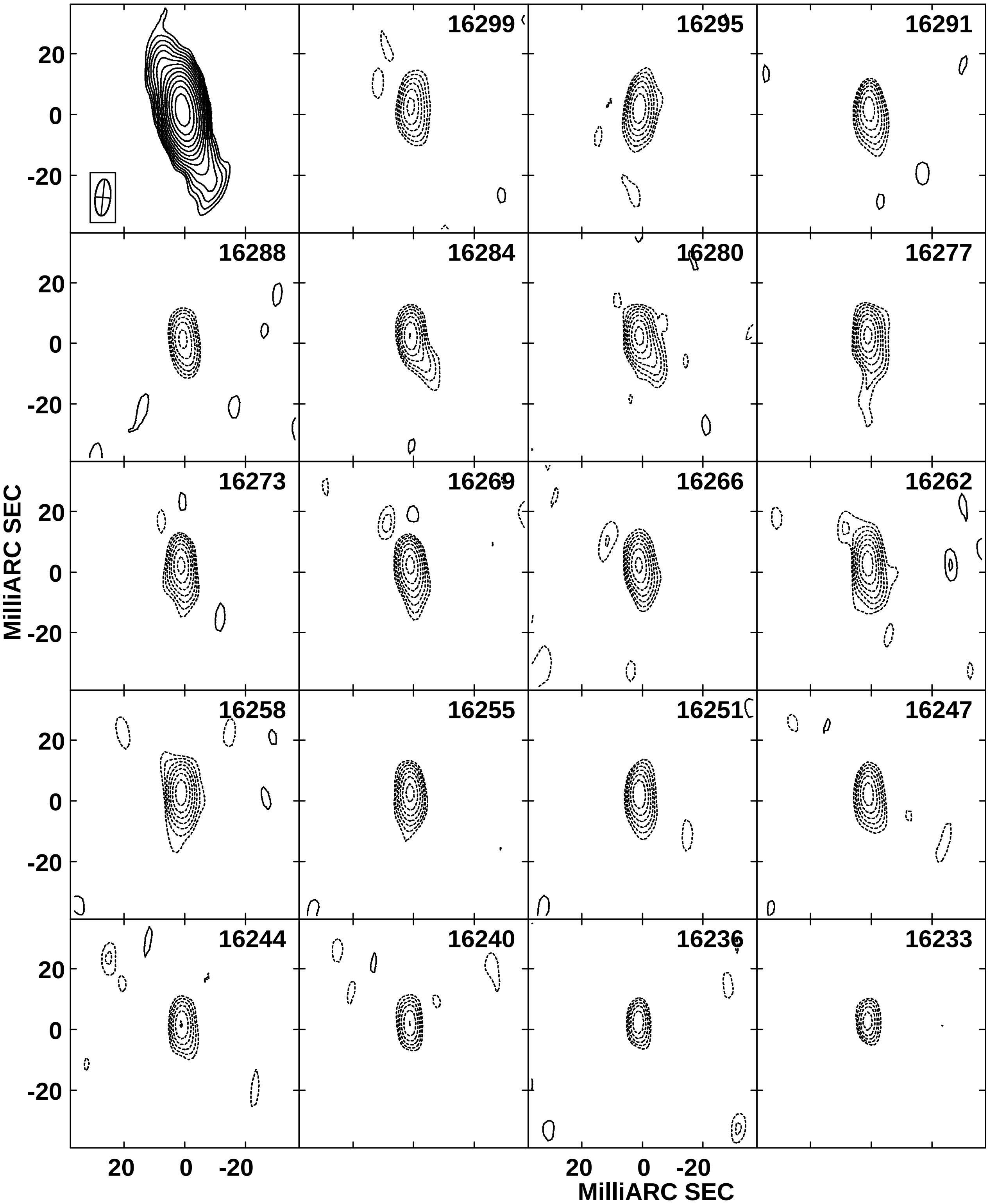

Fig. 6.— HI absorption in the central region of the spectrum in the nucleus of Hydra A. Contours are from the uniformly weighted continuum cube at −6, −8, −11, −16, −22, and −32 mJy/beam with a beam size of 14 × 6 mas in p.a. −5°. The peak absorption occurs at a velocity of 16,258 km s^{-1} (heliocentric and optical velocity definition with no relativistic correction). Each channel is separated by 3.67 km s^{-1}. The uniformly weighted continuum image at the same resolution is shown in the top left panel with contours starting at 1 mJy/beam and increasing by factors of root 2.

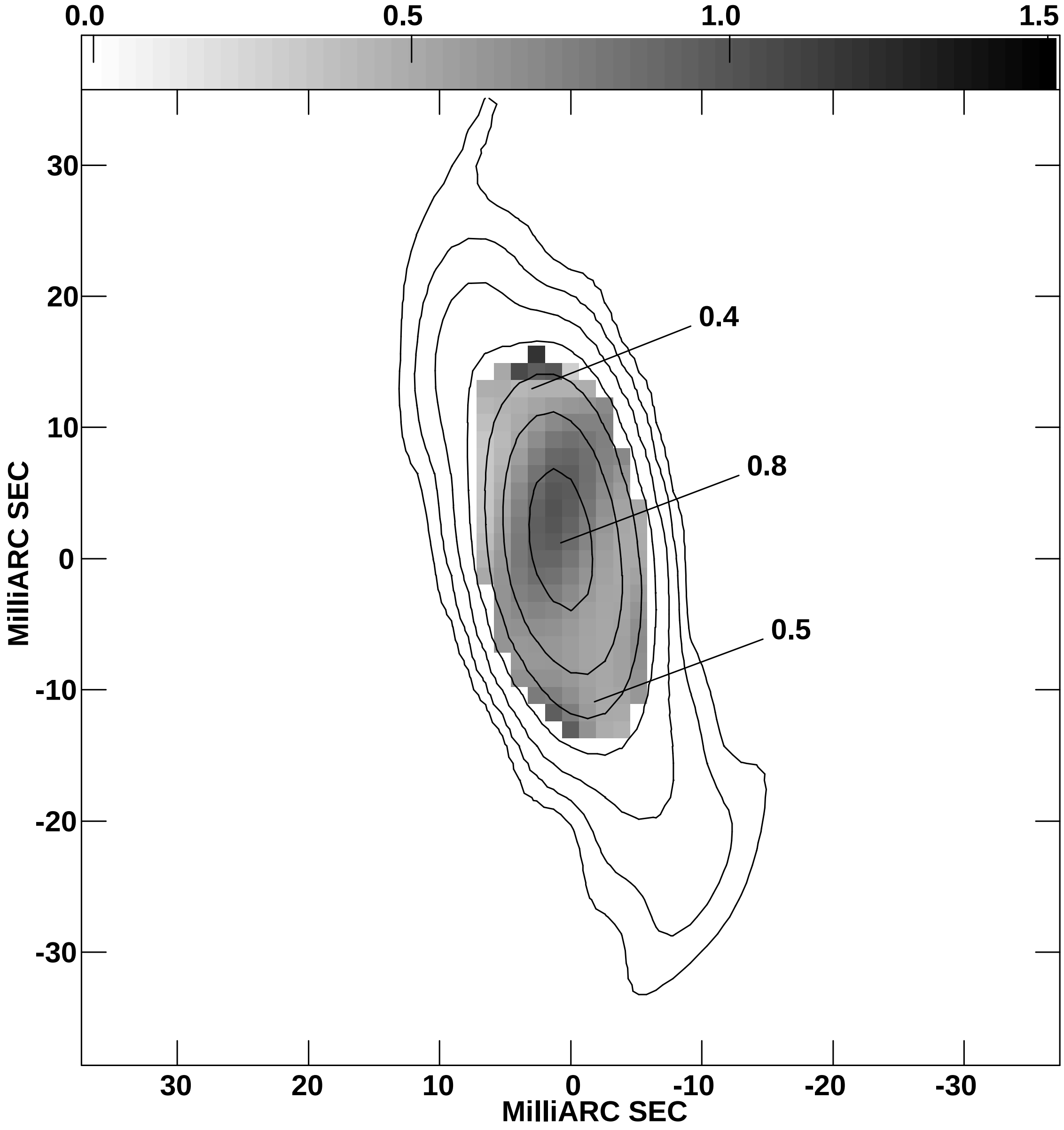

Fig. 7.— The optical depth map in Hydra A generated from Gaussian fits to the absorption line and from the continuum image. Contours are overlaid from the continuum map at 1, 2, 4, 8, 16, 32 and 64 mJy/beam. The grey scale ranges from τ between 0 and 1.5, and is only shown in the region with a high signal-to-noise in both the line and continuum.